applied sciences

MDPI

Article

Adsorption of Lead and Nickel on to Expanded Graphite Decorated with Manganese Oxide Nanoparticles

Quoc Cuong Do, Seonmi Choi, Hyojeon Kim and Seoktae Kang *

Department of Civil and Environmental Engineering, Korea Advanced Institute of Science and Technology (KAIST), 291 Daehak-ro, Yuseong-gu, Daejeon 34141, Korea; doquoccuong@kaist.ac.kr (Q.C.D.); csm891205@hanmail.net (S.C.); hyojeon73@kaist.ac.kr (H.K.)

* Correspondence: stkang@kaist.ac.kr; Tel.: +82-42-350-3635

Received: 3 November 2019; Accepted: 6 December 2019; Published: 9 December 2019

Abstract: In this study, expanded graphite (EG) was decorated with manganese oxide nanoparticles (MONPs) by the hydrothermal method, and the newly formed composite (MONPs-EG) was applied as adsorbent for the removal of heavy metals from aqueous solutions. The comparative and competitive adsorption of Pb^{2+} and Ni^{2+} (0.01–1.00 mM) on MONPs-EG was investigated. Data from isothermal adsorption of single and binary systems suggested that both Pb^{2+} and Ni^{2+} were well described by the Langmuir isotherm, and the maximum adsorption capacities at 298 K were calculated at 0.278 and 0.113 mmol/g for Pb^{2+} and Ni^{2+}, respectively. In binary systems, a dramatic decrease in adsorption capacity of Ni^{2+} was observed, while the adsorption capacity of Pb^{2+} was almost stable, indicating the favorable adsorption of Pb^{2+} over Ni^{2+} onto the prepared adsorbent. Kinetics studies of single and binary systems showed that a pseudo-second order model could explain the adsorption processes well. Thermodynamic analysis results demonstrated that the adsorption of these metal ions on the prepared adsorbent is spontaneous and exothermic in nature. The adsorption capacity of MONPs-EG increased significantly in the presence of humic acids. Overall, the results of this study suggest that MONPs-EG can be used effectively as an adsorbent for heavy metals removal from aqueous solutions.

Keywords: lead; nickel; adsorption; manganese oxide; expanded graphite; isotherms; kinetics; thermodynamics; partitioning coefficient

1. Introduction

With the growth of human activities, heavy metal contamination of soil and groundwater has become a great concern. Heavy metals are highly toxic and carcinogenic due to their persistence, bioaccumulation, and risk of reappearance according to changes of aquatic chemistry. Among various heavy metals, lead and nickel are considered the most dangerous contaminants when they are released into natural waters from various industrial activities including mining, leather processing, and metal plating. Lead can easily accumulate in human organs, causing anemia and severe damage to the nervous system, reproductive system, liver, brain, and kidneys [1]. Nickel is another toxic metal ion commonly present in steel and battery wastewater, causing vomiting, chest pain, and shortness of breath [2].

Various methods for heavy metal removal have been developed including reverse osmosis, ion exchange, electrodialysis, electrolysis, and adsorption. Among these technologies, adsorption has been acknowledged as a fast, inexpensive, and widely applicable technique [3–6]. In this regard, many studies have been focused on the effectiveness of various types of adsorbents, including biomass, clays, activated carbon, and metal particulates [7–10]. Among the listed adsorbents, adsorption onto natural

materials and biomass have been the most commonly tested techniques due to their cost-effectiveness when compared to those of other adsorbents such as metal particulates and activated carbon, while specific adsorption capacities have generally been found to be lower than that of metal particulates [7]. Moreover, effluent concentration for heavy metals during water treatment is very low in most cases, and the adsorption capacity is not the only criterion; the affinity between adsorbent and heavy metals should also be considered [1].

Nano-sized metal oxide particles have fascinated many researchers due to their high adsorption capacities as well as their extremely fast adsorption of and high affinity for heavy metals [11,12]. Among them, manganese oxide nanoparticles (MONPs), with notably high surface area and uniform size, are of great importance due to their novel applications in heavy metal removal [13,14]. However, due to the strong tendency of MONPs to form aggregates, synthesis of particles of well-controlled shape and size has been critical for maintaining their high affinity for heavy metals and their surface area. To minimize the aggregation of MONPs, various substrates with large surface area and uniform surface energy have been considered [15]. Specifically, graphene oxide (GO), a two-dimensional (2D) atomically thick carbon crystal with a honeycomb lattice, huge surface area, mechanical and thermal stability, and durability, has attracted great scientific and technological interest because of its potential applications in various areas including as a substrate for novel nano-particle deposition [16,17]. However, it is difficult to obtain homogeneous metal deposition on the hydrophobic surface because graphene sheets are not wetted by water, which leads to the infeasibility of traditional metal loading methods such as wet impregnation. Although GO is suitable and versatile, able to decorate various organic and inorganic chemicals, the subsequent reduction of GO to grow metal nanoparticles has been regarded as a complex, time-consuming, and highly toxic process [18,19]. Many efforts have been made to immobilize MONPs on various supporting materials such as sand, zeolite, and crushed brick [20–23], but their adsorption performance for heavy metals removal are still facing multiple challenges as discussed above.

Recently, several groups have investigated the use of expanded graphite (EG) because EG could achieve the requirements for nanoparticle support, including high porosity, large surface area, and low price [24,25]. Expanded graphite prepared from graphite intercalated compounds is a kind of hydrophobic carbon crystalline material with mainly macro- and mesopores; it has a unique worm-like structure [26,27], making it suitable as a support for nanoparticles such as MONPs. In addition, to the best of our knowledge, the combination of MONPs with EG for adsorptive removal of heavy metals has not been reported in literature.

In the present work, we introduced a facile and effective approach to uniformly immobilize MONPs on an expanded graphite surface; the newly formed composite (MONPs-EG) was then applied as an adsorbent for comparative and competitive removal of Pb^{2+} and Ni^{2+} in aqueous solution. Batch experiments were performed at various temperatures for a thermodynamic and kinetic study of the processes involved. The potential application of MONPs-EG composite material for the removal of heavy metals in the presence of humic acids (HA) was also investigated.

2. Materials and Methods

2.1. Material Preparation

2.1.1. Chemicals and Materials

Expandable graphite flakes (EXP-527) were supplied by Hyundai Coma Co., Seoul, Korea. Manganese(III) acetylacetonate or $Mn(acac)_3$ ($C_{15}H_{21}MnO_6$, 99.5%), manganese(II, III) oxide (Mn_3O_4, 97.0%), lead(II) nitrate (N_2O_6Pb, ≥99.0%), nickel(II) nitrate hexahydrate ($H_{12}N_2NiO_{12}$, 99.9%), methanol (CH_4O, 99.8%), and humic acid sodium salt (HA, technical grade) were purchased from Sigma-Aldrich Inc., Saint Louis, Missouri, United States.

2.1.2. Preparation of Manganese Oxide Nanoparticles-Expanded Graphite (MONPs-EG)

The graphite flakes was first expanded in a preheated muffle furnace (DMF-05, HumanLab Instrument Co., Gyeonggi, Korea) at 800 °C for 1 min to obtain EG. The prepared EG was then decorated with manganese oxide nanoparticles through a simple method using manganese acetylacetonate in the presence of methanol. In a typical experiment, 1.0 g EG and 0.5 g $Mn(acac)_3$ were loaded into a 450 mL Parr acid digression bomb (4767, Parr Instrument Co., Moline, Illinois, United States), followed by the addition of an appropriate amount of MeOH. The reaction mixture was carefully sealed and allowed to react at 300 °C for 10 min on an analog hot plate (HS-18, HumanLab Instrument Co., Gyeonggi-do, Korea). After cooling to room temperature, the solid composite was collected by vacuum filtration through a 1.0 μm membrane filter (JAWP, Merck KGaA, Darmstadt, Germany), thoroughly washed with ethanol, then dried overnight at 60 °C. Finally, the product was calcined at 350 °C for 4 h and was denoted MONPs-EG.

2.2. Material Characterization

Surface morphology of the prepared materials was observed using a scanning electron microscope (SEM, Stereoscan 440 FIB, LEO Electron Microscopy Ltd., Cambridge, United Kingdom) and transmission electron microscope (TEM, JEM-2100F, JEOL Ltd., Tokyo, Japan). An X-ray diffraction (XRD) study was carried out using an X-ray diffractometer (D8 advance, Bruker, Billerica, Massachusetts, United States) to examine the crystallographic property of the materials. The Brunauer-Emmett-Teller (BET) surface area and pore volume were measured by nitrogen adsorption/desorption isotherm method using a surface analyzer (MicrotracBEL Corp., Osaka, Japan).

2.3. Experiment

Batch adsorption experiments of Pb^{2+} and Ni^{2+} on the prepared MONPs-EG were carried out in single and binary metal systems. Adsorption isotherm experiments were studied with seven different concentrations of heavy metals ranging from 0.01 to 1.0 mM. The initial pH solution was adjusted to pH 5 using NaOH (0.1 M) and/or HCl (0.1 M). The experiments were performed using a fixed amount of MONPs-EG (0.5 g/L) for 100 mL metal solutions contained in series amber glass bottles, which were then shaken in an incubator (WIS-20, Daihan Scientific Co., Gangwon, Korea) for 12 h at a speed of 150 rpm and a temperature of 25 °C. The kinetic adsorption experiments studied 500 mL metal solutions of Pb^{2+} and/or Ni^{2+} prepared at initial concentrations of 0.1 and 0.01 mM, respectively. The experiment was performed for 4 h and samples were taken at given time intervals of the reaction, while other conditions were maintained the same as those in the isotherm experiments. In addition, to investigate the influence of natural organic matter on the adsorption behavior of the MONPs-EG, 10.0 mg/L humic acid was used. The concentration of metal ions in the solution was analyzed using inductively coupled plasma optical emission spectroscopy (Optima 7300 DV ICP-OES, Perkin Elmer Inc., Waltham, Massachusetts, United States), with method detection limits (MDL) of 1.7 μg/L and 0.5 μg/L for Pb^{2+} and Ni^{2+}, respectively.

The amount of metal adsorbed onto the prepared MONPs-EG (q_e) was calculated by subtracting the equilibrium concentrations of metal from the initial concentration, as expressed by the following Equation:

$$q_e = \frac{(C_0 - C_e)}{m} V \quad (1)$$

where C_0 and C_e are the initial and equilibrium concentrations of metals (mg/L), respectively, V is the volume of the solution (L), and m is the mass of the MONPs-EG (g).

2.4. Data Analysis

2.4.1. Adsorption Isotherms

The experimental equilibrium data of Pb^{2+} and Ni^{2+} adsorption onto the prepared MONPs-EG in single and binary metals systems were characterized using Langmuir and Freundlich isotherms [28–30]; their mathematical expressions are given by the following Equations (2) and (3), respectively.

$$q = q_{\max} \frac{K_L C_e}{1 + K_L C_e} \tag{2}$$

$$q = K_F {C_e}^{1/n} \tag{3}$$

where q_{max} is the maximum adsorption capacity of MONPs-EG for the metal ions (mmol/g), K_L is the Langmuir constant related to the affinity of the adsorption sites (L/mmol), K_F is the Freundlich constant related to the adsorption capacity (mmol/g) $(L/mmol)^{1/n}$, and *1/n* is the Freundlich constant related to the adsorption intensity (dimensionless).

The comparison between adsorption performances of the prepared MONPs-EG with its precursor or with various manganese oxide-based adsorbents were evaluated. In addition to adsorption capacity, we also investigated the partitioning coefficient (PC) of the adsorbent toward target adsorbate, which represents the ratio of the adsorbate amount in the solid adsorbent phase to its concentration in the liquid phase at equilibrium [31,32]. The *PC* can be calculated by the following Equation:

$$PC = \frac{q_e}{C_e} \tag{4}$$

where *PC* (mmol/g/mM) is the partitioning coefficient, q_e (mmol/g) is the adsorption capacity at equilibrium, and C_e (mM) is the concentration of metal ions at equilibrium.

2.4.2. Adsorption Kinetics

The kinetics of metal ions adsorption in single and binary system is also studied to determine the type of mechanism and the potential rate-controlling step of the processes. In the present study, two different reaction kinetic models (i.e., pseudo-first order and pseudo-second order) were applied to determine the kinetics of Pb^{2+} and Ni^{2+} on to the prepared MONPs-EG.

The pseudo-first order model was first presented by Lagergren in 1898 [33]; it has been widely used for adsorption kinetics study [34,35]. The equation can be expressed in non-linear and linear forms, as shown in Equations (5) and (6), respectively.

$$q_t = q_e(1 - e^{-k_1 t}) \tag{5}$$

$$\log(q_e - q_t) = \log q_e - \frac{k_1}{2.303} t \tag{6}$$

The pseudo-second order kinetic model was initially proposed by Blanchard et al. (1984) [36], and was then developed by Ho and McKay (1999) [37]. Its non-linear and linear forms can be expressed as shown in Equations (7) and (8), respectively.

$$q_t = \frac{q_e^2 k_2 t}{1 + k_2 q_e t} \tag{7}$$

$$\frac{t}{q_t} = \frac{1}{k_2 q_e^2} + \frac{1}{q_e} t \tag{8}$$

where q_e and q_t (mmol/g) are the adsorption capacities at equilibrium and at time t, respectively, k_1 (1/h) is the pseudo-first order rate constant, k_2 (g/mmol/h) is the pseudo-second order rate constant, and t (h) is the adsorption time.

2.4.3. Thermodynamic Analysis

The thermodynamic parameters of the adsorption process, such as the Gibbs free energy change (ΔG^0), enthalpy change (ΔH^0), and entropy change (ΔS^0) were analyzed through variations of the thermodynamic equilibrium constant (K_0) at the investigated temperatures (298, 308, and 323 K). In this work, K_0 values of the adsorption of metal ions onto the prepared MONPs-EG were calculated based on the method proposed by Biggar and Cheung (1973) [38], which can be defined as in the following Equation:

$$K_0 = \frac{a_s}{a_e} = \frac{\gamma_s}{\gamma_e}\frac{C_s}{C_e} \tag{9}$$

where a_s and γ_s are respectively the activity and activity coefficient of adsorbed metal ions on the MONPs-EG; a_e and γ_e are respectively the activity and activity coefficient of metal ions in the solution at equilibrium; C_s (mM) is the concentration of metal ions that adsorbed on the prepared adsorbent; and C_e (mM) is the concentration of metal ions in the solution at equilibrium.

When the concentration of metal ions in the solution approaches zero, resulting in $C_s \to 0$ and $C_e \to 0$, and the activity coefficients approach unity [38]. Equation (9) can be rewritten as:

$$\lim_{C_s \to 0} \frac{C_s}{C_e} = \frac{a_s}{a_e} = K_0 \tag{10}$$

The thermodynamic parameters were calculated as follows:

Gibbs free energy change of the adsorption process was directly estimated by Equation (11):

$$\Delta G^0 = -RT\ln(K_0) \tag{11}$$

where R is the universal gas constant (8.314 J/mol/K); and T (K) is the absolute solution temperature.

The Gibbs free energy change is a function of the change in enthalpy and entropy, which is expressed by Equation (12).

$$\Delta G^0 = \Delta H^0 - T\Delta S^0 \tag{12}$$

Combining Equations (11) and (12) resulted in Equation (13).

$$\ln(K_0) = -\frac{\Delta H^0}{R}\frac{1}{T} + \frac{\Delta S^0}{R} \tag{13}$$

ΔH^0 and ΔS^0 of the adsorption process will be, respectively, obtained from the slope ($-\Delta H^0/R$) and the intercept ($\Delta S^0/R$) of the plots of $\ln(K_0)$ as a function of $1/T$.

3. Results and Discussion

3.1. Material Property

SEM and TEM images of the prepared materials are presented in Figures 1 and 2. A comparison of the surface morphologies of these figures indicates that in the MONPs-EG composite each graphene sheet of EG was successfully decorated with nano-sized manganese oxide particles without significant change in structure. This is confirmed by the change in elemental compositions of samples before and after depositing manganese oxide on the EG surface (Table 1). The graphene sheets could be wetted by manganese oxide precursors due to the presence of supercritical methanol, which possesses near-zero surface tension and highly diffusive properties. The average diameter of the manganese oxide nanoparticles was measured at 23.5 ± 2.7 nm (n = 120). The specific surface area of EG decreased

slightly from 98.55 m^2/g to 87.60 m^2/g after the attachment of MONPs (Table 2); this decrease is attributed to augmentation of the material density [39]. Meanwhile, the average pore size increased from 6.20 nm to 13.91 nm, which might be due to the insertion and trapping of MONPs in the narrow pores between graphene sheets of the EG.

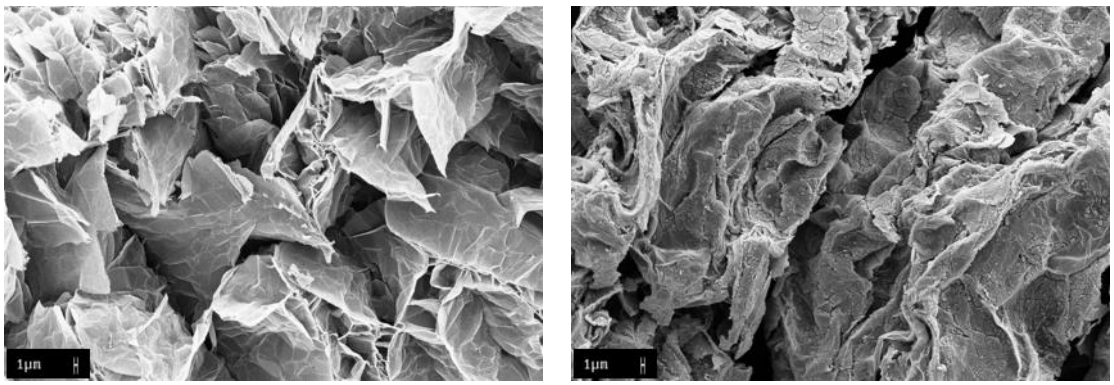

(**a**) (**b**)

Figure 1. Scanning electron microscope (SEM) images of: (**a**) expanded graphite (EG); (**b**) manganese oxide nanoparticles (MONPs)-EG composite.

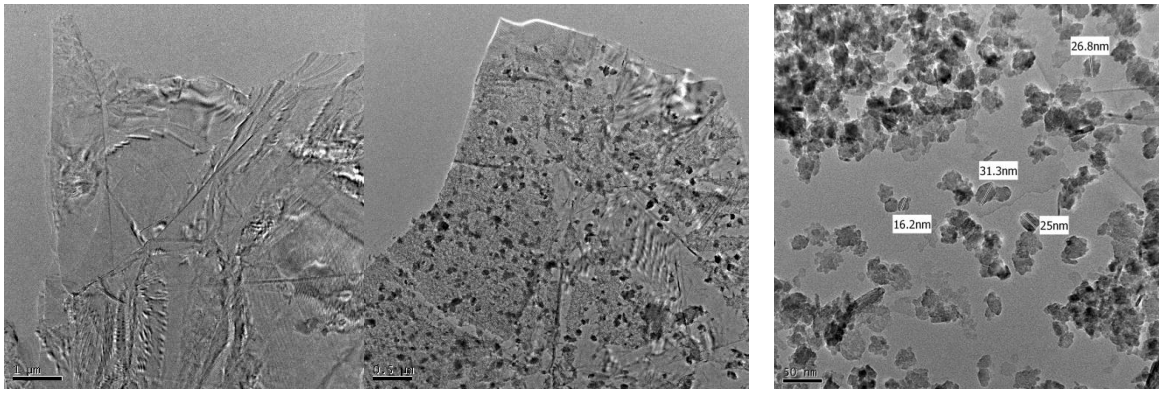

(**a**) (**b**) (**c**)

Figure 2. Transmission electron microscope (TEM) images of: (**a**) EG; (**b**) and (**c**) MONPs-EG composite at different magnifications.

Table 1. Elemental compositions of EG and MONPs-EG.

Element	Weight %		Atomic %	
	EG	MONPs-EG	EG	MONPs-EG
C	97.25	49.43	97.90	71.30
O	2.75	16.68	2.10	18.00
Mn	0	33.89	0	10.70

Figure 3 presents XRD patterns of EG, Mn_3O_4 nanoparticles, and MONPs-EG samples. The XRD pattern of EG exhibited typical diffraction peaks of graphite carbon around $2\theta = 26.5°$ and 54.5°, indicating the crystalline nature of the EG [40,41]. The MONPs-EG pattern revealed a relatively poor crystallinity in its structures compared to that of EG; the additional peaks at $2\theta = 18.0°$, 29.0°, 31.1°, 32.7°, 36.1°, 50.2°, and 60.0° are characteristic peaks of Mn_3O_4 (hausmannite), which can be observed from the XRD pattern of Mn_3O_4 nanoparticles.

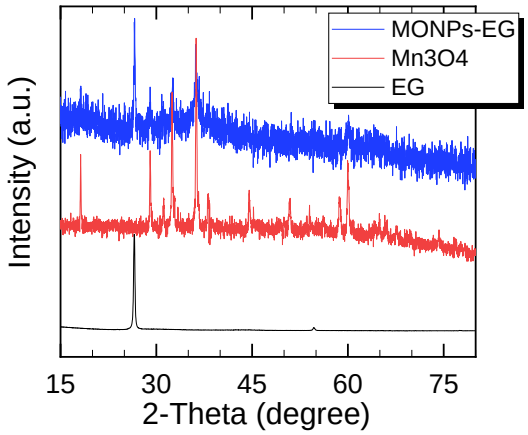

Figure 3. X-ray diffraction (XRD) patterns of EG, Mn_3O_4 nanoparticles, and MONPs-EG composite.

Table 2. Elemental compositions of EG and MONPs-EG.

Material	BET Surface Area (m^2/g)	Pore Volume (cm^3/g) [1]	Mean Pore Size (nm)
EG	98.55	0.16	6.20
MONPs-EG	87.60	0.13	13.91

[1] Pore volume was calculated at $P/P_0 = 0.990$.

3.2. Adsorption Isotherms

Experimental adsorption isotherm data for Pb^{2+} and Ni^{2+} on the prepared MONPs-EG in single and binary metals systems, and their fitting with the selected isotherm models, are presented in Figure 4. The corresponding parameters of the models are summarized in Table 3. The experimental data were better fitted to the Langmuir model, which provided much higher correlation coefficient values compared to those given by the Freundlich model, suggesting that the Langmuir model can effectively described the experimental results in both single and binary metals adsorption systems including the presence of HA. As a consequence, the estimated maximum adsorption capacities (q_{max}) agree well with the experimental data ($q_{max,\,exp.}$) at the highest level of initial metal concentrations.

The prepared MONPs-EG exhibited much higher adsorption capacity for Pb^{2+} than for Ni^{2+}. The maximum adsorption capacities at 298 K were calculated at 0.278 and 0.113 mmol/g for Pb^{2+} and Ni^{2+}, respectively. There is evidence that the effectiveness of an adsorption process is dependent on the size of the ions in the solution; higher ionic radius (or lower hydrated radius) of heavy metals generally led to higher maximum adsorption capacity [42–45]. In this respect, because the ionic radius of Pb^{2+} (119 pm) is larger than that of Ni^{2+} (70 pm), higher adsorption capacity of MONPs-EG for Pb^{2+} can be anticipated (Table 3). In addition, higher molecular weight metals (such as Pb) can be removed more easily than lower weight ones (such as Ni) [43].

In binary metal systems, the adsorption capacity of MONPs-EG for metal ions was reduced in the presence of other metal species (Figure 4). The numbers of heavy metal ions in binary systems are high compared to the availability of adsorption sites. It was observed that the removal efficiency of metal ions depends on the initial concentration and decrease as the initial metal ion concentration increases (Figure 4b). The maximum adsorption capacity of MONPs-EG for Pb^{2+} decreased slightly in the presence of the same level of Ni^{2+}. However, the MONPs-EG adsorption ability for Ni^{2+} was seriously inhibited when it coexisted with Pb^{2+} in the system. The maximum adsorption capacity for Ni^{2+} in a single metal system was 0.113 mmol/g, while it dropped to 0.021 mmol/g in the binary metal system. The existence of Pb^{2+} in the solution had a stronger impact on Ni^{2+} adsorption than vice versa. This suggested that competitive adsorption occurred when two metal ions coexisted in the solution.

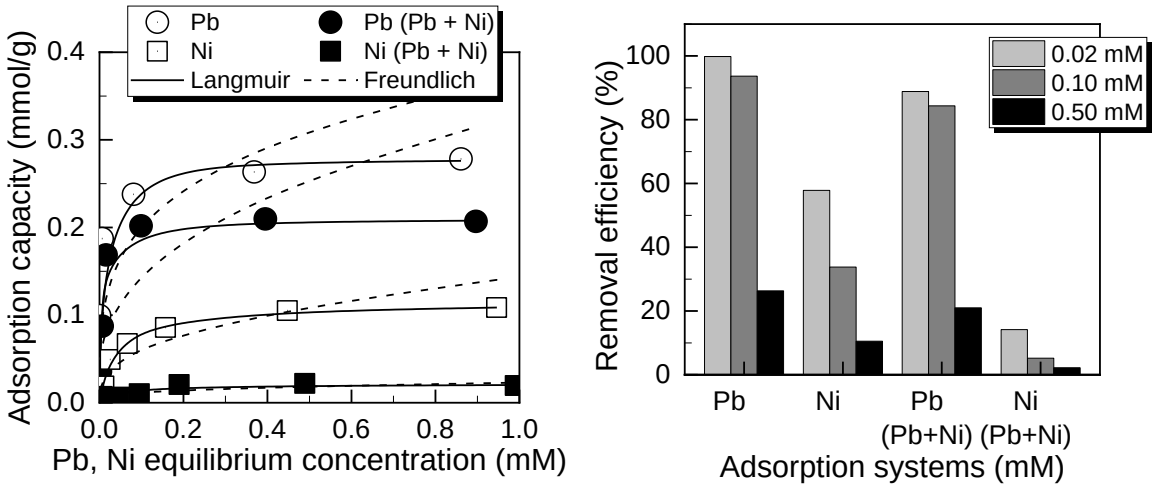

(**a**) (**b**)

Figure 4. (**a**) Adsorption isotherm of prepared MONPs-EG for metal ions; (**b**) heavy metals removal efficiencies at different initial concentrations in single and binary metals solutions.

Table 3. Adsorption isotherm parameters of prepared MONPs-EG in different metals solutions at 298 K.

Metal ion (System)	$q_{max, exp.}$ (mmol/g)	Langmuir Model			Freundlich Model		
		q_{max} (mmol/g)	K_L (L/mmol)	R^2	K_F (mmol/g) (L/mmol)$^{1/n}$	1/n	R^2
Pb	0.276	0.278	189.1	1	0.37	0.28	0.79
Pb (Pb + Ni)	0.207	0.209	174.2	1	0.33	0.32	0.81
Pb (Pb + HA)	0.297	0.298	217.0	1	0.40	0.27	0.61
Pb (Pb + Ni + HA)	0.219	0.220	186.8	1	0.30	0.26	0.67
Ni	0.110	0.113	26.5	1	0.14	0.36	0.91
Ni (Pb + Ni)	0.020	0.021	21.0	0.98	0.02	0.30	0.77
Ni (Ni + HA)	0.172	0.174	36.3	1	0.25	0.40	0.87
Ni (Pb + Ni + HA)	0.026	0.027	22.3	0.99	0.03	0.24	0.97

3.3. Adsorption Kinetics

Figure 5 elucidates the fitting of the pseudo-second order model with the experimental kinetics data of Pb^{2+} and Ni^{2+} adsorbed by the prepared MONPs-EG in single and binary metal systems. The adsorption of both metal ions occurred through two stages, a rapid stage in which most of the adsorption took place within 30 min of contact followed by a slow stage that lasted until the adsorption equilibrium had been reached. The adsorption processes gradually slowed down due to limitation in available active sites of adsorbent, which was supported by the decrease in metal removal efficiency at higher initial concentration (Figure 4b).

Pseudo-first order and pseudo-second order kinetic model fitting parameters are summarized in Table 4. The results show that the adsorption capacities ($q_{e, cal}$) of MONPs-EG for metals in all investigated systems, calculated by the pseudo-first order model, are quite different from those obtained experimentally ($q_{e, exp}$), while the values achieved from the pseudo-second order model are very close to the experimental data. In addition, the correlation coefficient values obtained from the pseudo-second order model are quite good ($R^2 > 0.99$) and much higher than those from the pseudo-first order model. These observations suggest that the pseudo-second order kinetic model can be used to better describe the kinetic mechanism of Pb^{2+} and Ni^{2+} adsorption on to the prepared

MONPs-EG. The pseudo-second order kinetic rate constant (k_2) values calculated for Pb^{2+} are much higher than those for Ni^{2+} in all systems (Table 4), implying that the adsorption of Pb^{2+} by MONPs-EG can occur more quickly and easily than can that of Ni^{2+}. These observations again confirm that MONPs-EG is capable of removing Pb^{2+} better than Ni^{2+} in aqueous solution.

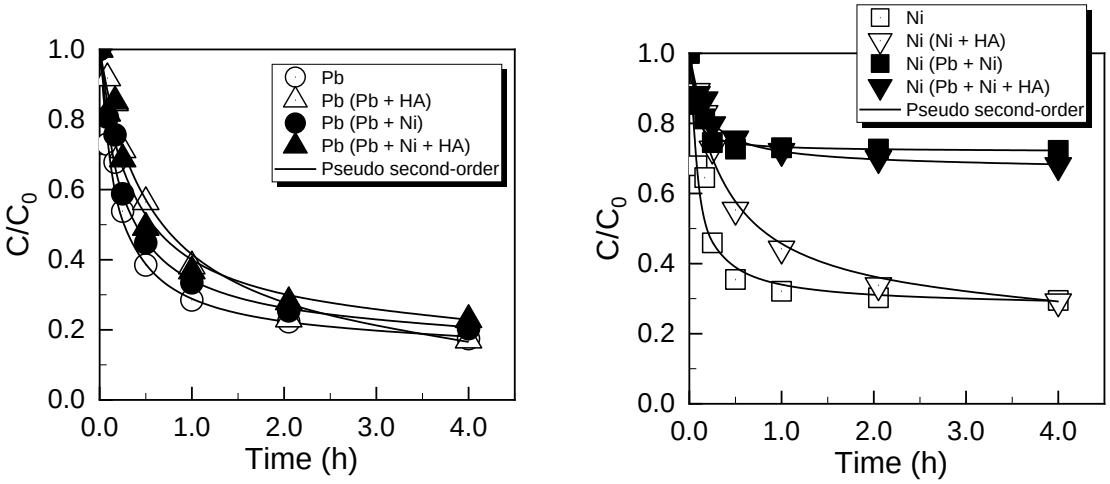

(**a**) (**b**)

Figure 5. Kinetic profiles of: (**a**) Pb^{2+}; (**b**) Ni^{2+} adsorption onto the prepared MONPs-EG in single and binary metal systems.

Table 4. Pseudo-first order and pseudo-second order kinetics parameters of prepared MONPs-EG in different metals solutions at 298 K.

Metal Ion (System)	$q_{e,exp.}$ (mmol/g)	Pseudo-First Order			Pseudo-Second Order		
		$q_{e,cal}$ (mmol/g)	k_1 (1/h)	R_1^2	$q_{e,cal}$ (mmol/g)	k_2 (g/mmol/h)	R_2^2
Pb	0.187	0.114	0.49	0.80	0.171	32.96	1
Pb (Pb+Ni)	0.169	0.111	0.39	0.90	0.168	24.37	1
Pb (Pb+HA)	0.190	0.152	0.53	0.90	0.191	9.19	0.99
Pb (Pb+Ni+HA)	0.170	0.121	0.59	0.87	0.168	16.73	0.99
Ni	0.015	0.006	0.61	0.73	0.014	875.98	1
Ni (Pb+Ni)	0.007	0.003	0.25	0.66	0.006	4486.45	1
Ni (Ni+HA)	0.015	0.011	0.72	0.93	0.016	168.52	1
Ni (Pb+Ni+HA)	0.008	0.005	0.34	0.72	0.007	991.41	1

3.4. Thermodynamic Study

The effects of temperature on the adsorption capacities of MONPs-EG for Pb^{2+} and Ni^{2+} were investigated through a series of experiments at 298 K, 308 K, and 323 K in single metal solutions. The results are shown in Figure 6. The adsorption capacities were found to decrease with the increase of temperature, suggesting that the adsorption of metal ions onto MONPs-EG was favorable at low temperature. At higher temperature, the attractive forces between MONPs-EG and metal ions could be weakened, leading to a decrease in adsorption capacity. Thermodynamic studies were performed to determine the nature of the adsorption processes; the calculated parameters are summarized in Table 5. The negative values of ΔH^0 confirm the exothermic nature of the adsorption of both metal ions onto the prepared adsorbent in single metal systems at 298–323 K [46,47], which is supported by the results of the temperature effect on the adsorption processes. Negative values of ΔS^0 reflected that the randomness decreases at the MONPs-EG and solution interface during the adsorption of metal

ions [48,49]. The higher magnitude of ΔS^0 obtained in the Pb^{2+} system signified that it had a better affinity toward and was more stable on the MONPs-EG compared to Ni^{2+}. Furthermore, negative values of ΔG^0 at all investigated temperatures indicated that the adsorptions of both metal ions onto the prepared MONPs-EG were thermodynamically favorable and spontaneous in nature [28,50].

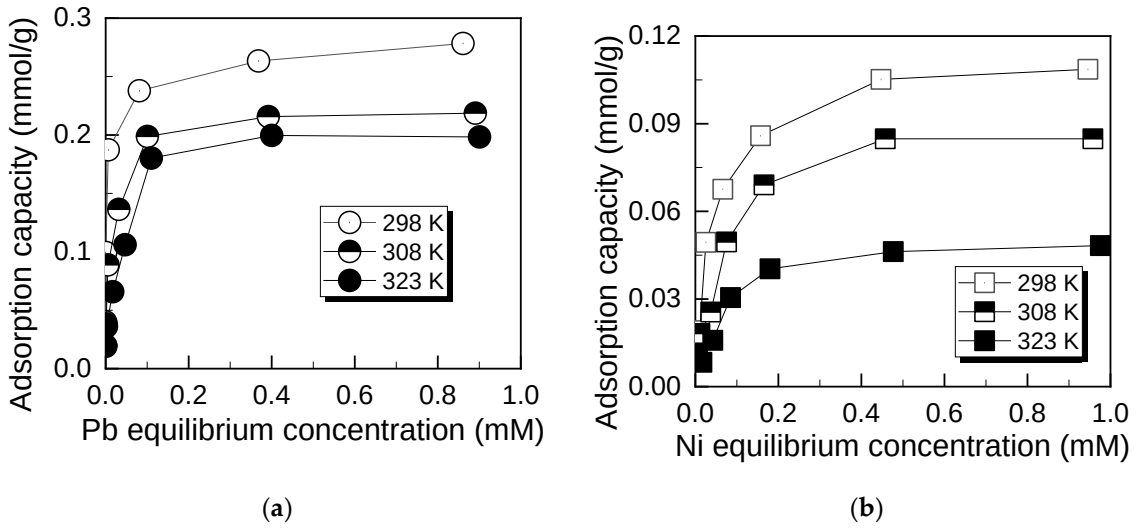

(**a**) (**b**)

Figure 6. Effect of temperature on adsorption behaviors of prepared MONPs-EG for: (**a**) Pb^{2+}; (**b**) Ni^{2+} in single metal solutions.

Table 5. Thermodynamic parameters of adsorption of Pb^{2+} and Ni^{2+} onto the prepared MONPs-EG in single systems.

Metal ion	Temperature (K)	$\ln K_0$	ΔG^0 (kJ/mol)	ΔS^0 (kJ/mol/K)	ΔH^0 (kJ/mol)
Pb^{2+}	298	14.42	−35.16	−0.27	−115.65
	308	12.21	−31.90		
	323	10.47	−27.82		
Ni^{2+}	298	8.92	−21.83	−0.08	−46.68
	308	8.04	−20.81		
	323	7.32	−19.54		

3.5. Effect of Humic Acids (HA)

Humic acids (HA) are the major components of dissolved organic matter in natural surface water. They can have excellent binding characteristics and electrostatic interactions with metal ions in solution, leading to the formation of metal-organic complexes, which might affect the adsorption of metal ions on the prepared adsorbent [51–53]. The effect of HA on the adsorption behaviors of metal ions onto the prepared MONPs-EG in single and binary systems are shown in Figures 5 and 7. It can be seen that the presence of HA in the systems reduced the adsorption rates of metals ions onto the MONPs-EG. This reduction is clearly observed for single metal systems, while it is indistinct in binary metal systems (Figure 5). However, with the supporting data shown in Table 4, the changes in the adsorption rates are noticeable in binary metal systems with the coexistence of HA. Indeed, wide variations in the pseudo-second order kinetic rate constants (k_2) are observed in these systems, which are decreased from 24.37 to 16.73 and 4486.45 to 991.41 (g/mmol/h) for Pb^{2+} and Ni^{2+}, respectively. Interestingly, despite the fact that the adsorption rate is hindered with the presence of HA, the adsorption capacity was promoted, especially in single systems (Figure 7). The maximum adsorption capacity of MONPs-EG for Pb^{2+} in single metal systems was 0.278 mmol/g at 298 K; this value increased to 0.298 mmol/g in the presence of 10 mg/L HA (Table 3). A similar trend was observed for Ni^{2+}: the adsorption capacity increased from 0.113 to 0.174 mmol/g when HA coexists in the system. The presence of HA in

binary metal systems can also promote the overall adsorption process, but increases in the adsorption capacities of MONPs-EG in these cases are insignificant, probably due to adsorption competition between metal ions, as discussed above. However, the results also verified the positive effect of HA coexistence in the systems on overall adsorption processes. The increase of metal ion adsorption capacities in the presence of HA might be due to the chelation of Pb^{2+} and Ni^{2+} with functional groups on HA, and adsorption of HA onto exposed carbon and manganese oxides structure on the MONPs-EG composite [53–56].

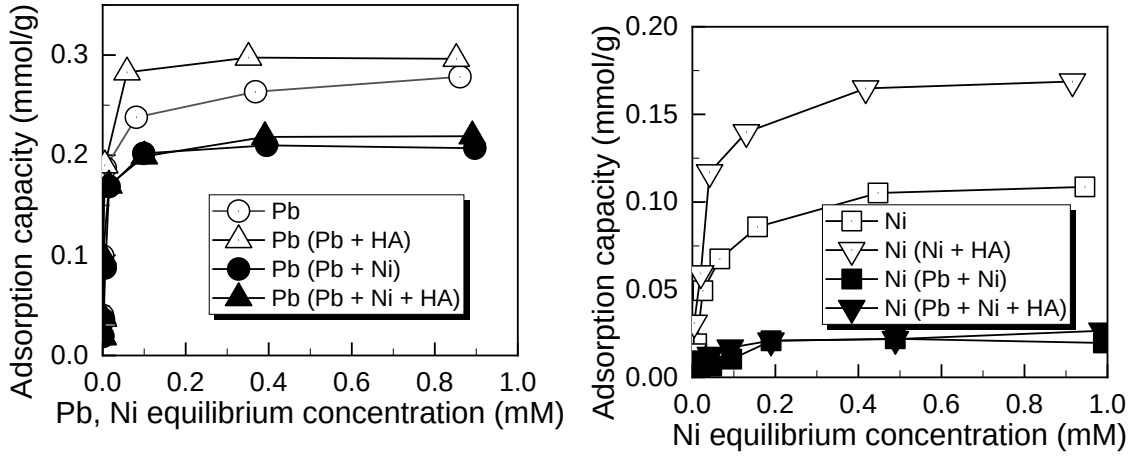

(**a**) (**b**)

Figure 7. Effect of humic acids (HA) on adsorption behaviors of MONPs-EG for: (**a**) Pb^{2+}; (**b**) Ni^{2+} in single and binary metal solutions.

The comparison of adsorption performances of Pb^{2+} and Ni^{2+} by the prepared MONPs-EG achieved in this study with other similar adsorbents under various experimental conditions are presented in Table 6. The MONPs-EG exhibited superior adsorption capacities, which are much higher than those of previous studies that used various adsorbent such as expanded graphite (EG) and its modifications (G-EG, P-EG) [57], manganese oxide-coated sand (MOCS) [21,24], manganese oxide coated crushed brick (MOCB) [21], and manganese oxide-coated zeolite (MOCZ) [22,23]. This finding suggested the applicability of the coating process and the prepared MONPs-EG can serve as a competent adsorbent for removing heavy metals from the aquatic environment. Regarding the partition coefficient (PC), the higher value of PC is generally referred to as a good adsorption affinity [32,57]. However, our results found that the PC values are inversely proportional to the initial metals concentration in solution. This mean that the higher affinity of metal ions towards the MONPs-EG could be achieved at lower initial concentration. Therefore, an outstanding adsorption affinity might not necessarily correspond to an excellent adsorption capacity. The partition coefficients obtained in this study are comparable to the results of previous studies with various adsorbents although there are distinct differences in adsorption capacities between them (Table 6). The magnitude of the computed PC values is generally higher when the initial concentration loaded on to the batch system becomes lower due to the enhanced efficiency of adsorptive processes. However, the occurrences of exceptionally high PC value for Pb^{2+} at the lowest initial concentration of 0.10 mM are still somewhat unusual. It may possibly be attributed to the unusually preferential removal of Pb^{2+} under the initial conditions which considerably stimulated the interaction between the adsorbate (Pb^{2+}) and the adsorbent (MONPs-EG). The strong affinity of Pb^{2+} to MONPs-EG over that of Ni^{2+} can also be ascribable in terms of thermodynamic consideration in that the magnitude of ΔG^0 was significantly higher in Pb^{2+} than in Ni^{2+} (Table 5).

Table 6. Adsorption behaviors of Pb^{2+} and Ni^{2+} in single systems by various adsorbents.

Metal Ion	Adsorbent	C_o (mM)	pH	Temp. (K)	Ce (mM)	q_e (mmol/g)	PC (mmol/g/mM)	Reference
Pb^{2+}	MOCS	0.53	5.0	293	0.021	0.026	1.240	[20]
	MOCB	0.53	5.0	293	0.021	0.023	1.100	[20]
	MOCZ	2.42	5.5	296	0.520	0.190	0.370	[21]
	MOCS	3.38	4.0	288	2.700	0.240	0.090	[22]
	MOCZ	1.54	4.0	295	1.360	0.008	0.006	[23]
	MONPs-EG	0.10	5.0	298	0.006	0.187	31.167	This study
	MONPs-EG	0.50	5.0	298	0.368	0.263	0.715	This study
	MONPs-EG	1.00	5.0	298	0.861	0.276	0.321	This study
Ni^{2+}	EG	0.17	-	295	0.164	0.007	0.043	[58]
	G-EG	0.17	-	295	0.163	0.009	0.055	[58]
	P-EG	0.17	-	295	0.157	0.013	0.083	[58]
	MONPs-EG	0.10	5.0	298	0.066	0.068	1.030	This study
	MONPs-EG	0.50	5.0	298	0.447	0.105	0.235	This study
	MONPs-EG	1.00	5.0	298	0.946	0.110	0.116	This study

4. Conclusions

Manganese oxides were successfully decorated onto the surface of expanded graphite, and the newly formed composite MONPs-EG was employed as adsorbent for the removal of heavy metals from aqueous solution. The adsorption isotherms were well described by the Langmuir model, and the maximum adsorption capacity of MONPs-EG in a single metal system at 298 K can attain values of 0.278 and 0.113 mmol/g for Pb^{2+} and Ni^{2+}, respectively. The adsorption capacity values for individual metal ions were reduced by coexistence with another metal, indicating substantial competition between the metal ions for binding sites on the prepared MONPs-EG. The adsorption of both Pb^{2+} and Ni^{2+} onto the prepared MONPs-EG followed the pseudo-second order kinetic model. The adsorption processes were spontaneous and exothermic in nature, which were inhibited with increase in temperature. The presence of humic acids in the systems significantly increased the adsorption of metal ions on to the prepared adsorbent. This study suggests that MONPs-EG can be effectively used as an adsorbent for heavy metal removal from aqueous solution.

Author Contributions: Conceptualization, S.K. and Q.C.D.; methodology, Q.C.D. and S.C.; validation, S.K. and Q.C.D.; formal analysis, Q.C.D. and S.C.; investigation, S.C. and H.K.; data curation, Q.C.D.; writing—original draft preparation, Q.C.D.; writing—review and editing, Q.C.D. and S.K.; supervision, S.K.; project administration, S.K.; funding acquisition, S.K.

Funding: This research was funded by Korea Ministry of Land, Infrastructure and Transport (MOLIT) as "Innovative Talent Education Program for Smart City".

Conflicts of Interest: The authors declare no conflict of interest. The funders had no role in the design of the study; in the collection, analyses, or interpretation of data; in the writing of the manuscript; or in the decision to publish the results.

References

1. Vukovic, G.D.; Marinkovic, A.D.; Skapin, S.D.; Ristic, M.D.; Aleksic, R.; Peric-Grujic, A.A.; Uskokovic, P.S. Removal of lead from water by amino modified multi-walled carbon nanotubes. *Chem. Eng. J.* **2011**, *173*, 855–865. [CrossRef]
2. Alandis, N.M.; Aldayel, O.A.; Mekhemer, W.K.; Hefne, J.A.; Jokhab, H.A. Thermodynamic and Kinetic Studies for the Adsorption of Fe(III) and Ni(II) Ions from Aqueous Solution Using Natural Bentonite. *J. Dispers. Sci. Technol.* **2010**, *31*, 1526–1534. [CrossRef]
3. Sulaymon, A.H.; Ebrahim, S.E.; Mohammed-Ridha, M.J. Equilibrium, kinetic, and thermodynamic biosorption of Pb(II), Cr(III), and Cd(II) ions by dead anaerobic biomass from synthetic wastewater. *Environ. Sci. Pollut. Res.* **2013**, *20*, 175–187. [CrossRef] [PubMed]

4. Naddafi, K.; Nabizadeh, R.; Saeedi, R.; Mahvi, A.H.; Vaezi, F.; Yaghmaeian, K.; Ghasri, A.; Nazmara, S. Biosorption of lead(II) and cadmium(II) by protonated Sargassum glaucescens biomass in a continuous packed bed column. *J. Hazard. Mater.* **2007**, *147*, 785–791. [CrossRef] [PubMed]
5. Do, Q.C.; Kim, M.S.; Kim, D.; Ko, S.O.; Kang, S. Sustainable harvesting of aqueous phase fatty acids by expanded graphite and isopropyl alcohol. *Int. J. Hydrog. Energy* **2016**, *41*, 21780–21786. [CrossRef]
6. Do, Q.C.; Chungman, M.; Seokoh, K.; Seoktae, K.; Am, J.; Kim, D.H. Hydrothermal decoration of iron oxide nanoparticles on expanded graphite for adsorptional of phosphorus. In Proceedings of the 2015 IEEE 15th International Conference on Nanotechnology (IEEE-NANO), Rome, Italy, 27–30 July 2015; pp. 258–261.
7. Saharan, P.; Chaudhary, G.R.; Mehta, S.K.; Umar, A. Removal of Water Contaminants by Iron Oxide Nanomaterials. *J. Nanosci. Nanotechnol.* **2014**, *14*, 627–643. [CrossRef]
8. Singh, S.; Barick, K.C.; Bahadur, D. Functional Oxide Nanomaterials and Nanocomposites for the Removal of Heavy Metals and Dyes. *Nanomater. Nanotechnol.* **2013**, *3*, 1–19. [CrossRef]
9. Mudhoo, A.; Garg, V.K.; Wang, S.B. Removal of heavy metals by biosorption. *Environ. Chem. Lett.* **2012**, *10*, 109–117. [CrossRef]
10. Sdiri, A.T.; Higashi, T.; Jamoussi, F. Adsorption of copper and zinc onto natural clay in single and binary systems. *Int. J. Environ. Sci. Technol.* **2014**, *11*, 1081–1092. [CrossRef]
11. Hua, M.; Zhang, S.J.; Pan, B.C.; Zhang, W.M.; Lv, L.; Zhang, Q.X. Heavy metal removal from water/wastewater by nanosized metal oxides: A review. *J. Hazard. Mater.* **2012**, *211*, 317–331. [CrossRef]
12. Karvelas, E.; Liosis, C.; Benos, L.; Karakasidis, T.; Sarris, I. Micromixing Efficiency of Particles in Heavy Metal Removal Processes under Various Inlet Conditions. *Water* **2019**, *11*, 1135. [CrossRef]
13. Kumar, S.; Nair, R.R.; Pillai, P.B.; Gupta, S.N.; Iyengar, M.A.R.; Sood, A.K. Graphene Oxide-$MnFe_2O_4$ Magnetic Nanohybrids for Efficient Removal of Lead and Arsenic from Water. *ACS Appl. Mater. Interfaces* **2014**, *6*, 17426–17436. [CrossRef] [PubMed]
14. Kim, E.J.; Lee, C.S.; Chang, Y.Y.; Chang, Y.S. Hierarchically Structured Manganese Oxide-Coated Magnetic Nanocomposites for the Efficient Removal of Heavy Metal Ions from Aqueous Systems. *ACS Appl. Mater. Interfaces* **2013**, *5*, 9628–9634. [CrossRef] [PubMed]
15. Kim, E.J.; Kim, J.; Choi, S.C.; Chang, Y.S. Sorption behavior of heavy metals on poorly crystalline manganese oxides: Roles of water conditions and light. *Environ. Sci. Processes Impacts* **2014**, *16*, 1519–1525. [CrossRef] [PubMed]
16. Zhao, J.; Xue, H.; Zhang, L.; Yu, J.H.; Hu, H.Q. Decoration of ultrafine platinum-ruthenium particles on functionalized graphene sheets in supercritical fluid and their electrocatalytic property. *J. Nanopart. Res.* **2012**, *14*, 935. [CrossRef]
17. Geim, A.K.; Novoselov, K.S. The rise of graphene. *Nat. Mater.* **2007**, *6*, 183–191. [CrossRef]
18. Li, Y.; Fan, X.B.; Qi, J.J.; Ji, J.Y.; Wang, S.L.; Zhang, G.L.; Zhang, F.B. Gold nanoparticles-graphene hybrids as active catalysts for Suzuki reaction. *Mater. Res. Bull.* **2010**, *45*, 1413–1418. [CrossRef]
19. Si, Y.; Samulski, E.T. Synthesis of water soluble graphene. *Nano Lett.* **2008**, *8*, 1679–1682. [CrossRef]
20. Boujelben, N.; Bouzid, J.; Elouear, Z. Removal of Lead(II) Ions from Aqueous Solutions Using Manganese Oxide-Coated Adsorbents: Characterization and Kinetic Study. *Adsorpt. Sci. Technol.* **2009**, *27*, 177–191. [CrossRef]
21. Irannajad, M.; Haghighi, H.K. Removal of Co^{2+}, Ni^{2+}, and Pb^{2+} by Manganese Oxide-Coated Zeolite: Equilibrium, Thermodynamics, and Kinetics Studies. *Clays Clay Miner.* **2017**, *65*, 52–62. [CrossRef]
22. Zou, W.; Han, R.; Chen, Z.; Shi, J.; Liu, H. Characterization and Properties of Manganese Oxide Coated Zeolite as Adsorbent for Removal of Copper(II) and Lead(II) Ions from Solution. *J. Chem. Eng. Data* **2006**, *51*, 534–541. [CrossRef]
23. Han, R.; Lu, Z.; Zou, W.; Wang, D.; Shi, J.; Yang, J. Removal of copper(II) and lead(II) from aqueous solution by manganese oxide coated sand: II. Equilibrium study and competitive adsorption. *J. Hazard. Mater.* **2006**, *137*, 480–488. [CrossRef] [PubMed]
24. Afanasov, I.M.; Shornikova, O.N.; Avdeev, V.V.; Lebedev, O.I.; Van Tendeloo, G.; Matveev, A.T. Expanded graphite as a support for Ni/carbon composites. *Carbon* **2009**, *47*, 513–518. [CrossRef]
25. Shi, P.H.; Zhu, S.B.; Zheng, H.G.; Li, D.X.; Xu, S.H. Supported Co_3O_4 on expanded graphite as a catalyst for the degradation of Orange II in water using sulfate radicals. *Desalin. Water Treat.* **2014**, *52*, 3384–3391. [CrossRef]

26. Li, S.; Tian, S.; Feng, Y.; Lei, J.; Wang, P.; Xiong, Y. A comparative investigation on absorption performances of three expanded graphite-based complex materials for toluene. *J. Hazard. Mater.* **2010**, *183*, 506–511. [CrossRef] [PubMed]
27. Vieira, F.; Cisneros, I.; Rosa, N.G.; Trindade, G.M.; Mohallem, N.D.S. Influence of the natural flake graphite particle size on the textural characteristic of exfoliated graphite used for heavy oil sorption. *Carbon* **2006**, *44*, 2590–2592. [CrossRef]
28. Do, Q.C.; Kang, S. Thermodynamic analysis of fatty acid harvesting by novel carbon-based adsorbent. *Environ. Sci. Pollut. Res.* **2016**, *23*, 7146–7154. [CrossRef]
29. Langmuir, I. The adsorption of gases on plane surface of glass, mica and platinum. *J. Am. Chem. Soc.* **1918**, *40*, 1361–1403. [CrossRef]
30. Freundlich, H. Über die absorption in lösungen. *Z. Für Phys. Chem.* **1906**, *57*, 385–470.
31. Vikrant, K.; Kim, K.-H. Nanomaterials for the adsorptive treatment of Hg(II) ions from water. *Chem. Eng. J.* **2019**, *358*, 264–282. [CrossRef]
32. Kim, K.-H.; Szulejko, J.E.; Raza, N.; Kumar, V.; Vikrant, K.; Tsang, D.C.W.; Bolan, N.S.; Ok, Y.S.; Khan, A. Identifying the best materials for the removal of airborne toluene based on performance metrics-A. critical review. *J. Clean. Prod.* **2019**, *241*, 118408. [CrossRef]
33. Lagergren, S. About the theory of so-called adsorption of soluble substances. *Kungliga Svenska Vetenskapsakademiens Handlingar* **1898**, *24*, 1–39.
34. Taty-Costodes, V.C.; Fauduet, H.; Porte, C.; Delacroix, A. Removal of Cd(II) and Pb(II) ions, from aqueous solutions, by adsorption onto sawdust of Pinus sylvestris. *J. Hazard. Mater.* **2003**, *105*, 121–142. [CrossRef] [PubMed]
35. Tran, T.N.; Kim, D.G.; Ko, S.O. Adsorption Mechanisms of Manganese (II) Ions onto Acid-treated Activated Carbon. *KSCE J. Civ. Eng.* **2018**, *22*, 3772–3782. [CrossRef]
36. Blanchard, G.; Maunaye, M.; Martin, G. Removal of heavy metals from waters by means of natural zeolites. *Water Res.* **1984**, *18*, 1501–1507. [CrossRef]
37. Ho, Y.S.; McKay, G. Pseudo-second order model for sorption processes. *Process Biochem.* **1999**, *34*, 451–465. [CrossRef]
38. Biggar, J.W.; Cheung, M.W. Adsorption of Picloram (4-Amino-3, 5, 6-Trichloropicolinic Acid) on Panoche, Ephrata, and Palouse Soils: A Thermodynamic Approach to the Adsorption Mechanism1. *Soil Sci. Soc. Am. J.* **1973**, *37*, 863–868. [CrossRef]
39. Do, Q.C.; Kim, D.G.; Ko, S.O. Catalytic activity enhancement of a Fe_3O_4@SiO_2 yolk-shell structure for oxidative degradation of acetaminophen by decoration with copper. *J. Clean. Prod.* **2018**, *172*, 1243–1253. [CrossRef]
40. Hatui, G.; Malas, A.; Bhattacharya, P.; Dhibar, S.; Kundu, M.K.; Kumar Das, C. Effect of expanded graphite and PEI-co-Silicon Rubber on the thermo mechanical, morphological as well as rheological properties of in situ composites based on poly (ether imide) and liquid crystalline polymer. *J. Alloys Compd.* **2015**, *619*, 709–718. [CrossRef]
41. Malas, A.; Das, C.K.; Das, A.; Heinrich, G. Development of expanded graphite filled natural rubber vulcanizates in presence and absence of carbon black: Mechanical, thermal and morphological properties. *Mater. Des.* **2012**, *39*, 410–417. [CrossRef]
42. Mobasherpour, I.; Salahi, E.; Pazouki, M. Comparative of the removal of Pb^{2+}, Cd^{2+} and Ni^{2+} by nano crystallite hydroxyapatite from aqueous solutions: Adsorption isotherm study. *Arabian J. Chem.* **2012**, *5*, 439–446. [CrossRef]
43. Hossain, M.A.; Ngo, H.H.; Guo, W.S.; Nghiem, L.D.; Hai, F.I.; Vigneswaran, S.; Nguyen, T.V. Competitive adsorption of metals on cabbage waste from multi-metal solutions. *Bioresour. Technol.* **2014**, *160*, 79–88. [CrossRef] [PubMed]
44. Osińska, M. Removal of lead(II), copper(II), cobalt(II) and nickel(II) ions from aqueous solutions using carbon gels. *J. Sol Gel Sci. Technol.* **2017**, *81*, 678–692. [CrossRef]
45. Gao, Z.; Bandosz, T.J.; Zhao, Z.; Han, M.; Qiu, J. Investigation of factors affecting adsorption of transition metals on oxidized carbon nanotubes. *J. Hazard. Mater.* **2009**, *167*, 357–365. [CrossRef]
46. Hu, Q.; Gao, D.W.; Pan, H.; Hao, L.; Wang, P. Equilibrium and kinetics of aniline adsorption onto crosslinked sawdust-cyclodextrin polymers. *RSC Adv.* **2014**, *4*, 40071–40077. [CrossRef]

47. Sepehr, M.N.; Al-Musawi, T.J.; Ghahramani, E.; Kazemian, H.; Zarrabi, M. Adsorption performance of magnesium/aluminum layered double hydroxide nanoparticles for metronidazole from aqueous solution. *Arabian J. Chem.* **2017**, *10*, 611–623. [CrossRef]
48. Gao, Q.; Liu, F.; Zhang, T.; Zhang, J.; Jia, S.; Yu, C.; Jiang, K.; Gao, N. The Role of Lactic Acid Adsorption by Ion Exchange Chromatography. *PLoS ONE* **2010**, *5*, e13948. [CrossRef]
49. Chen, P.; Zhang, H.; Liu, H.; Luo, X.; Lin, X.; Lu, X.; Tang, Y. Cost effective biochar gels with super capabilities for heavy metal removal. *RSC Adv.* **2016**, *6*, 75430–75439. [CrossRef]
50. Crini, G. Kinetic and equilibrium studies on the removal of cationic dyes from aqueous solution by adsorption onto a cyclodextrin polymer. *Dyes Pigments* **2008**, *77*, 415–426. [CrossRef]
51. Sounthararajah, D.P.; Loganathan, P.; Kandasamy, J.; Vigneswaran, S. Effects of Humic Acid and Suspended Solids on the Removal of Heavy Metals from Water by Adsorption onto Granular Activated Carbon. *Int. J. Environ. Res. Public Health* **2015**, *12*, 10475–10489. [CrossRef]
52. Chen, J.P.; Wu, S. Simultaneous adsorption of copper ions and humic acid onto an activated carbon. *J. Colloid Interface Sci.* **2004**, *280*, 334–342. [CrossRef] [PubMed]
53. Do, Q.C.; Kim, D.G.; Ko, S.O. Insights into heterogeneous Fenton-like systems catalyzed by novel magnetic yolk-shell structures for the removal of acetaminophen from aquatic environments. *J. Water Process Eng.* **2019**, *32*, 100980. [CrossRef]
54. Basu, H.; Saha, S.; Mahadevan, I.A.; Pimple, M.V.; Singhal, R.K. Humic acid coated cellulose derived from rice husk: A novel biosorbent for the removal of Ni and Cr. *J. Water Process Eng.* **2019**, *32*, 100892. [CrossRef]
55. Vermeer, A.W.P.; McCulloch, J.K.; van Riemsdijk, W.H.; Koopal, L.K. Metal Ion Adsorption to Complexes of Humic Acid and Metal Oxides: Deviations from the Additivity Rule. *Environ. Sci. Technol.* **1999**, *33*, 3892–3897. [CrossRef]
56. Kerndorff, H.; Schnitzer, M. Sorption of metals on humic acid. *Geochim. Cosmochim. Acta* **1980**, *44*, 1701–1708. [CrossRef]
57. Al-Wabel, M.; Elfaki, J.; Usman, A.; Hussain, Q.; Ok, Y.S. Performance of dry water- and porous carbon-based sorbents for carbon dioxide capture. *Environ. Res.* **2019**, *174*, 69–79. [CrossRef]
58. Jiang, L.; Zhang, J.; Xu, X.; Zhang, J.; Liu, H.; Guo, Z.; Kang, Y.; Li, Y.; Xu, J. Characterization and application of expanded graphite modified with phosphoric acid and glucose for the removal of Ni(II) from aqueous solution. *Appl. Surf. Sci.* **2015**, *357*, 2355–2363. [CrossRef]